# Preparation and characterization of CeO$_2$/Al-MCM-41 catalysts and its effect on NO conversion efficiency

## Renjing Qiao[1], Qi Xu[1*] and Kaige Chen[2]

[1]*School of Chemistry and Chemical Engineering, Jiangsu University, Zhenjiang, Jiangsu Province, China*
[2]*School of Petroleum Engineering, Changzhou University, Changzhou, Jiangsu Province, China*

_____

**ABSTRACT**

*The NH$_3$-SCR activity of Al-MCM-41 modified with cerium dioxide (CeO$_2$/Al-MCM-41) is investigated under simulated flue gas. X-ray diffractogram (XRD), Brunauer-Emmett-Teller (BET), and transmission electron microscopy (TEM) analyses are employed to characterize the samples. The effects of CeO$_2$ loading value, reaction temperatures, and individual flue gas components, including O$_2$ and SO$_2$, on the NO conversion efficiency are investigated. The experimental results show that the NO conversion efficiency can be significantly improved by CeO$_2$ and, at a reaction temperature of 350 ºC, the optimal loaded mass percentage of CeO$_2$ is 8 %. As the reaction temperature is increased from 200 to 350 ºC, NO conversion efficiency increases markedly, but decreases above 350 ºC. In addition, the presence of O$_2$ has positive effects on the NO conversion efficiency, while the presence of SO$_2$ has inhibited effects.*

**Keywords:** selective catalytic reduction(SCR), CeO$_2$, CeO$_2$/Al-MCM-41, NO conversion efficiency, simulated flue gas.

_____

**INTRODUCTION**

Nitrogen oxides (NOx) generally include 95 % NO and 5 % NO$_2$, contributing towards negative environmental impacts such as photochemical smog, acid rain, ozone depletion, and greenhouse effects[1,2]. Nitrogen oxides are mainly emitted from the combustion of fossil fuels in power stations and automobiles. Currently, the selective catalytic reduction (SCR) has been confirmed as one of the most effective approach for the control of NOx emission from fuel gas[3-4]. The well-known commercial catalysts are consist of TiO$_2$ as support material and V$_2$O$_5$ or V$_2$O$_5$-WO$_3$ (MoO$_3$) as active catalytic components ,which has excellent activity in the SCR reaction within a narrow temperature range (300-400 ºC)[5,6]. However, these catalysts suffer from severe disadvantages: the toxicity of vanadium, easy deactivation caused by fly ash, SO$_2$ and H$_2$O in the flue gas and low specific surface areas of TiO$_2$[7].

Because of these disadvantages of the present catalysts, many researchers focus on developing efficient and stable NH$_3$-SCR catalysts. In recent years, much attention has been paid to Ce-based SCR catalysts[8-10], which attributes to its high oxygen storage/release capacity and the ability of shift between Ce$^{4+}$ and Ce$^{3+}$ under oxidizing or reducing conditions[11-13]. In addition, since the discovery of mesoporous molecular sieves (M41S) by scientists, the mesoporous materials have attracted considerable interest because of regular pore channels and large surface areas [14-18]. There into, aluminosilicate M41S materials have been the focus of researches because the tetrahedrally coordinated Al can produce active sites for adsorption, ion exchange and catalysis [19-21].

In this study, we synthesize Al-MCM-41 from pretreated attapulgite as silica and aluminum sources without addition of silica or aluminum reagents according to a novel method[22], and evaluate the NO conversion efficiency of CeO$_2$ impregnated Al-MCM-41 in a lab-scale fixed-bed system. The simulated flue gas system included N$_2$, O$_2$, SO$_2$, NO

_____

and $NH_3$. During the course of the experiment, different operating conditions, including loading values of $CeO_2$, reaction temperatures and flue gas components on the NO conversion efficiency are discussed.

## EXPERIMENTAL SECTION

**Catalyst preparation**
Attapulgite is firstly mixed with solid NaOH at mass ratio of 1:1.5. The mixture is heated at 600 °C for 2 h, subsequently dispersed in deionized water by stirring and then aged at room temperature for 24 h. The supernatant is used as the Si and Al source without addition of Si or Al reagents. 1 g cetyltrimethylammonium bromide ( CTAB ) and 1 g polyethylenglycol 4000 ( PEG4000 ) are dissolved in 50 mL of deionized water, then added 80 mL of supernatant. The mixed solution is constantly stirred for 1 h at 30 °C, adjusted pH value of the mixed solution to 9.0 with diluted HCl solution (2 mol/L). After pH adjustment, the white mixed solution is stirred at 30 °C for 1 h and transferred into a teflon-lined steel autoclave and heated at 110 °C for 48 h. The resultant product is filtered, washed and dried at 80 °C for 12 h to produce the as-synthesized material. The as-synthesized material is calcined at 550 °C for 6h in air at a heating rate of 2 °C/min to remove the template and produce the white powder of Al-MCM-41.

To produce $CeO_2$/Al-MCM-41 using wet impregnation method. Firstly, $Ce(NO_3)_3 \cdot 6H_2O$ is dissolved in deionized water to form different concentrations of $Ce(NO_3)_3$ solution. Then, 2 g Al-MCM-41 is added to 10 ml solution with stirring in a proportion corresponding to different loading values (the mass ratio of $CeO_2$/ Al-MCM-41) varying from 4 to 10 wt %. The samples are subsequently dried at 120 °C to vaporize the water completely. Finally, the powder mixture is calcined at 500 °C in air for 5 h to produce 4, 6, 8, and 10 wt% $CeO_2$/Al-MCM-41 composites.

**Catalyst Characterization**
X-ray diffractogram (XRD) measurements are carried out with Rigaku D/max 2500PC using Cu Kα radiation to determine the crystalline structure of the catalyst. $N_2$ adsorption-desorption isotherms are measured at 77K using Quantachrome Autosorb- iQ-TCD System. The Brunauer-Emmett-Teller (BET) method is used to calculate the specific surface area and the total pore volume. The pore size distribution curves of the catalysts are characterized using the Barret-Joyner -Halenda (BJH) formula. The transmission electron microscopy (TEM) images are obtained on JEOL JEM-2100 microscope operating at 200 kV.
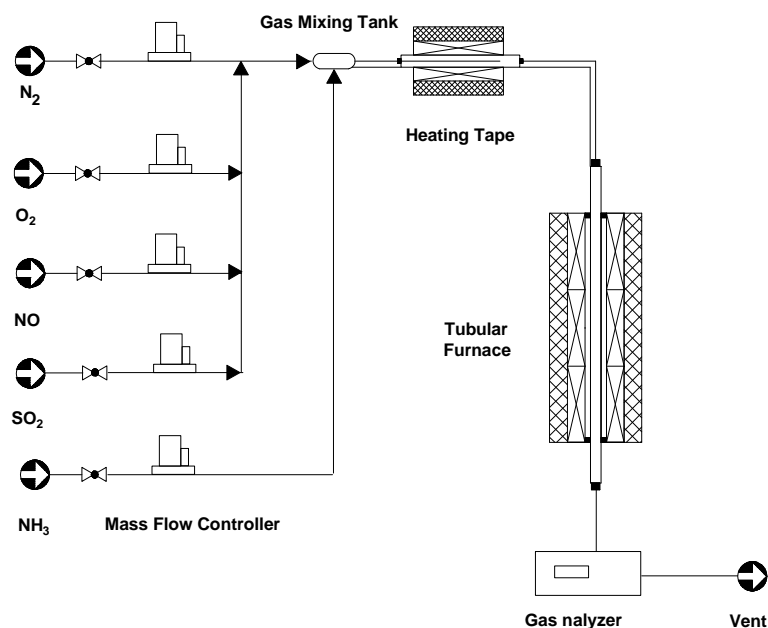


**Fig1. Schematic diagram of the experimental setup**

**Catalyst activity measurement.**
A schematic diagram of the experimental setup is shown in Fig.1 The apparatus consisted of a simulated flue gas system, a fixed-bed reactor, and a gas analyzer system including an fuel gas analyser. The simulated flue gas includes 5 vol% $O_2$, 1000 ppm NO, 1200 ppm $SO_2$ and the balance gas $N_2$. The total flow is controlled at 1 L/min in eachexperiment, corresponding to a gas hour space velocity (GHSV) of 35000 $h^{-1}$.

The fixed-bed reactor is comprised of a quartz tube with an inner diameter of 10 mm and a digital temperature controller. About 3 mL of the catalyst is packed in the quartz tube. The concentrations of NO are continually

_____

monitored by a flue gas analyzer (Germany VarioPlus Ind). During the experiment, the activity of the catalyst is determined after 1 h reaction time before the concentration analysis. For the whole tests, the NO conversion efficiency is defined as flollow.

$$\text{NO conversion (\%)}=\frac{\text{NO}_{in}-\text{NO}_{out}}{\text{NO}_{in}}\times 100 \tag{1}$$

$NO_{in}$ is the inlet NO concentration of the quartz tube and $NO_{out}$ is the outlet NO concentration of the quartz tube.

## RESULTS AND DISCUSSION

**Sample characteristics**
The XRD patterns of Al-MCM-41 and $CeO_2$/Al-MCM-41 are showed in Fig.2 The peaks at the ranges of $2\theta = 15–40°$ in the XRD patterns are corresponding to the specific peaks of Al-MCM-41, which can be detected in Al-MCM-41, 4% $CeO_2$/Al-MCM-41 and 6%$CeO_2$/Al-MCM-41. However, there are no the specific peaks of Al-MCM-41 in 8% $CeO_2$/Al-MCM-41 and 10%$CeO_2$/Al-MCM-41, which is caused by relatively lower crystallinity of Al-MCM-41 compared with $CeO_2$. Meanwhile, there are no apparent characteristic peaks ascribable to $CeO_2$ in 4% $CeO_2$/Al-MCM-41, which indicates that $CeO_2$ is highly dispersed on the surface of Al-MCM-41. Nevertheless, a weak crystal phase of $CeO_2$ is detected at $2\theta = 28.5°$, $47.4°$ and $56.3°$ for 6% $CeO_2$/Al-MCM-41, 8% CeO2/Al-MCM-41 and 10% $CeO_2$/ Al-MCM-41 in the XRD patterns, powerfully indicating that the surface of Al-MCM-41 is occupied by $CeO_2$ as the $CeO_2$ loading increases to somewhere between 6% and 10%.
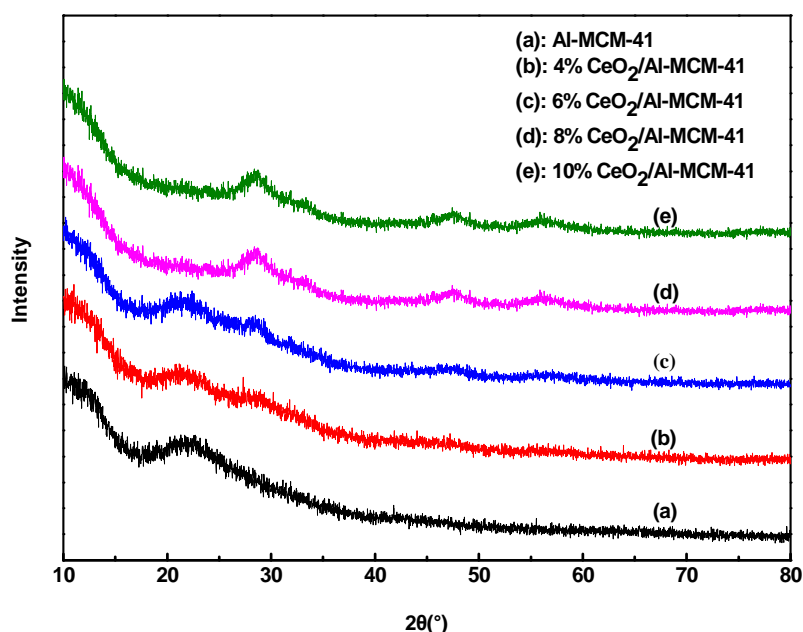


**Fig2. XRD patterns of Al-MCM-41 and CeO₂/Al-MCM-41**

$N_2$ adsorption-desorption isotherms of Al-MCM-41 and $CeO_2$/Al-MCM-41 are showed in Fig.3 The isotherms are of the typical type IV shape, which is the characteristic adsorption type of typical mesoporous materials. $N_2$ adsorption capacity increases significantly and a small hysteresis loop at relative pressure of 0.3-0.5, which originates from $N_2$ capillary condensation in the pores, indicating that these samples are mesoporous. When relative pressure is close to 0.9, adsorption capacity of isotherms also increases sharply and exist a large hysteresis loop, representing the capillary condensation of $N_2$ in the particles.

_____
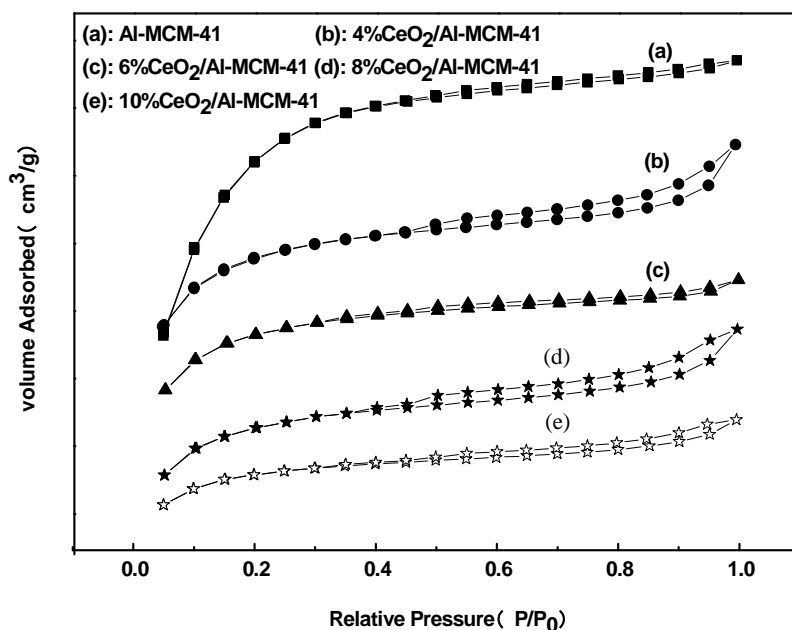


**Fig3. N$_2$ adsorption-desorption isotherms of Al-MCM-41 and CeO$_2$/Al-MCM-41**

The pore structure parameters of Al-MCM-41 and CeO$_2$/Al-MCM-41 are listed in Table 1. It is obvious that the Al-MCM-41 has the highest BET surface area value of 945.76 m$^2$/g, largest total pore volume value of 0.86 cm$^3$/g and pore size value of 3.86 nm. However, with the increase of the CeO$_2$ loading value, the BET surface area, total pore volume and pore size of CeO$_2$/Al-MCM-41 samples decrease. Especially, when the CeO$_2$ loading value reaches 8 %, the BET surface area is sharply reduced from 945.76 to 373.35 m$^2$/g, the total pore volume is reduced from 0.86 to 0.38 m$^3$/g, and the pore size chanes from 3.86 to 2.54 nm. The reason may be due to that the existence of active component, CeO$_2$, over the external surface of Al-MCM-41 causes destruction of the thin pore walls and blocking.

**Table1. Surface area, pore volume and pore diameter of Al-MCM-41 and Ce- Al-MCM-41**

| Samples | BET surface area (m$^2$/g) | total pore volume (cm$^3$/g) | Pore size (nm) |
|---|---|---|---|
| Al-MCM-41 | 945.76 | 0.86 | 3.86 |
| 4% CeO$_2$/Al-MCM-41 | 498.17 | 0.41 | 2.92 |
| 6% CeO$_2$/Al-MCM-41 | 421.86 | 0.39 | 2.65 |
| 8% CeO$_2$/Al-MCM-41 | 373.35 | 0.38 | 2.54 |
| 10% CeO$_2$/Al-MCM-41 | 318.12 | 0.35 | 2.24 |

The transmission electron microscopy (TEM) patterns of 8 % CeO$_2$/Al-MCM-41 (Fig.4) indicate that the CeO$_2$ particles are dispersed uniformly and the size is about 1.8 nm. These results clearly indicate that the CeO$_2$ nanoparticles are successfully loaded on the surface of Ce/Al-MCM-41.
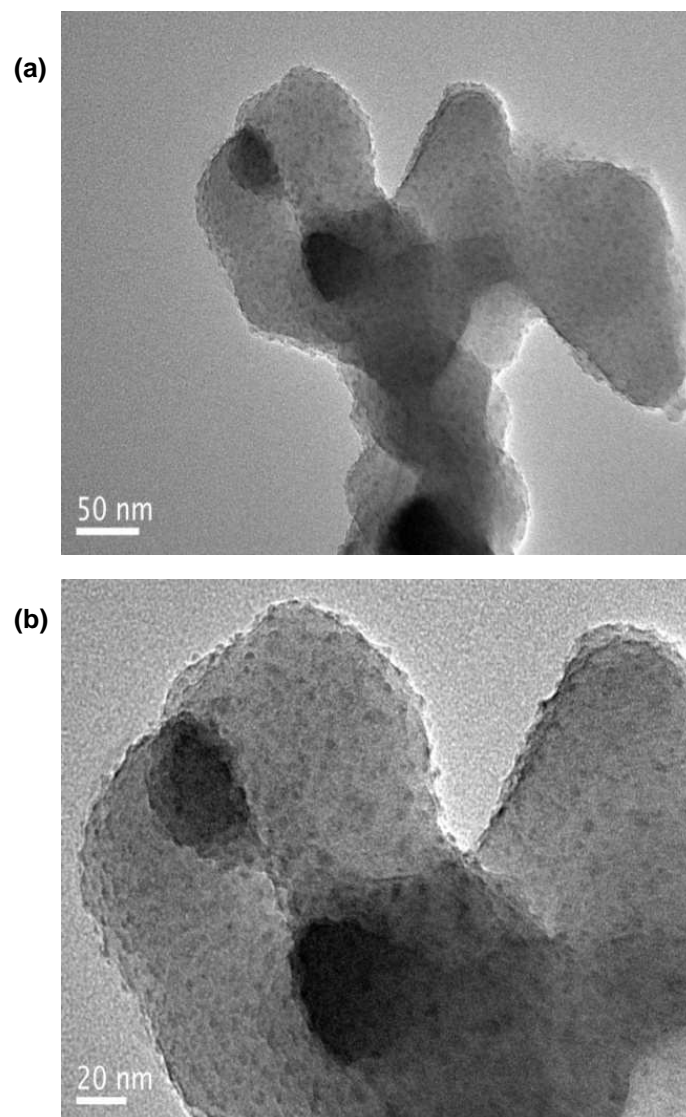
**Fig4. TEM images of CeO₂ / Al-MCM-41**

**Effects of CeO₂ Loading Value and Reaction Temperature**

To find the optimal CeO₂ loading value, NO conversion efficiency as a function of temperature is compared in Fig.5 over Al-MCM-41 and CeO₂/Al-MCM-41 catalysts with different CeO₂ loading values(4, 6, 8, and 10 wt %). The pure Al-MCM-41 demonstrates notably little NO conversion efficiency, and the best conversion efficiency in the entire temperature range is 18.6 %. However, Al-MCM-41 impregnation with CeO₂ can increase the NO conversion efficiency significantly, particularly when the loading value is 8 %. At the temperature of 350 °C, with CeO₂ loading value supported on Al-MCM-41 increasing from 4 to 8 wt %, NO conversion efficiency increases from 39.8 % to 68.6 %. However, further increasing CeO₂ loading values resultes in the decrease of NO conversion efficiency. When CeO₂ loading value increases above 8 wt %, NO conversion efficiency of Al-MCM-41 impregnation with CeO₂ decreases. When the loading value is 10 %, the NO conversion efficiency decreases to 49.4 %. The possible reason can be ascribed to the fact that the surface area, total pore volume, and pore size of CeO₂/Al-MCM-41 decrease with the increase of CeO₂ as shown in Table 1. The decrease of the surface area prevents the valid collision between NO and CeO₂/Al-MCM-41[23]. Therefore, the result indicates that the optimal CeO₂ value is 8% for NO conversion efficiency, which can be ascribed to the greater amount of chemisorbed oxygen on the surface resulted from $Ce^{3+}$ on the sorbent surface[24]. Moreover, when the CeO₂ loading value is kept constant, NO conversion efficiency increases with temperature from 200 to 350 °C and then decreases dramatically when the temperature further increased from 350 to 400 °C. This is because when the temperature exceeds 350 °C, the excessive CeO₂ would react with SO₂ and O₂, forming Ce(SO₄)₂ [25]

$$CeO_2 + 2SO_2 + O_2 \rightarrow Ce(SO_4)_2 \tag{2}$$
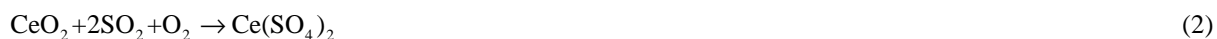
The generated $Ce(SO_4)_2$ covers the surface of Al-MCM-41 and blocks its pores, preventing NO from contacting $CeO_2$. Moreover, with the temperature increasing, the cell size of crystal $CeO_2$ becomes larger and can also block the pores of Al-MCM-41[26]. These changes lead to a decrease of NO conversion efficiency.
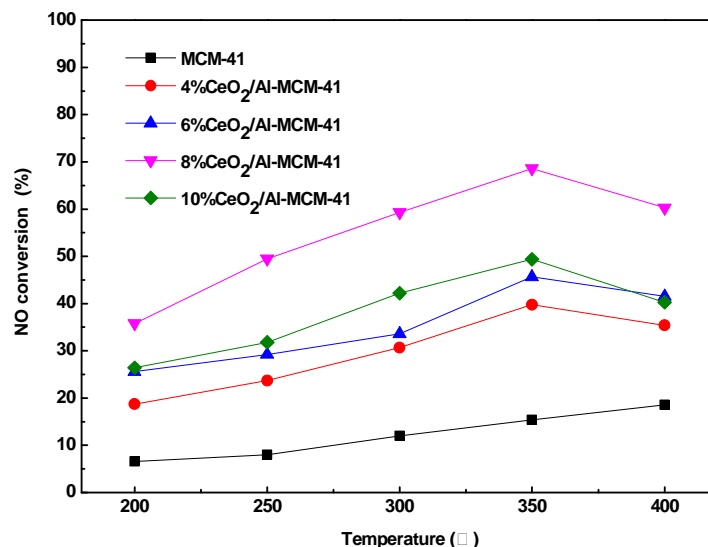


**Fig5. Relationship between the NO conversion and $CeO_2$ loading value supported on Al-MCM-41 at different reaction temperatures**

**Effect of $O_2$**

Fig.6 shows the effects of different $O_2$ concentrations (0, 4, and 8 %) in the flue gas on NO conversion efficiency over the 8% $CeO_2$/Al-MCM-41 at 350 ℃ (reaction time = 1 h). The result reveals that NO conversion efficiency only achieves about 43.6 % in the absence of $O_2$. With the concentration of $O_2$ increases, the NO conversion efficiency enhances. It indicates that $O_2$ has a positive effect on the NO conversion efficiency over $CeO_2$/Al-MCM-41.
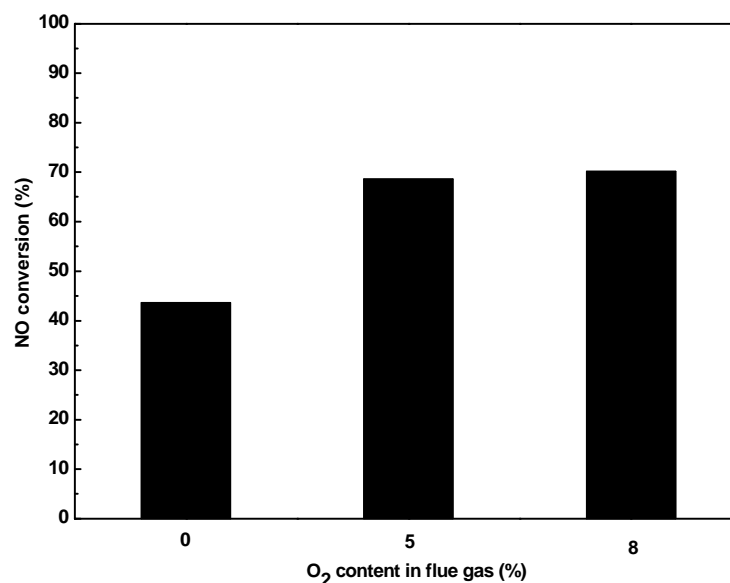


**Fig.6 Effect of the $O_2$ concentration on the NO conversion of 8% $CeO_2$/Al-MCM-41**

**Effect of $SO_2$.**

Fig.7 shows the effects of $SO_2$ in the flue gas on the NO conversion efficiency of 8 % $CeO_2$/Al-MCM-41 at 350 ℃ (reaction time = 1 h) in the presence of $SO_2$ (300-900 ppm). The result reveals that $SO_2$ has an inhibitory effect on NO conversion efficiency over $CeO_2$/Al-MCM-41. At the reaction temperature of 350 ℃, the NO conversion efficiency can reach 68.6 % with 300 ppm $SO_2$, but decreases to 56.8 % with 900 ppm $SO_2$ in the simulated flue gas system.
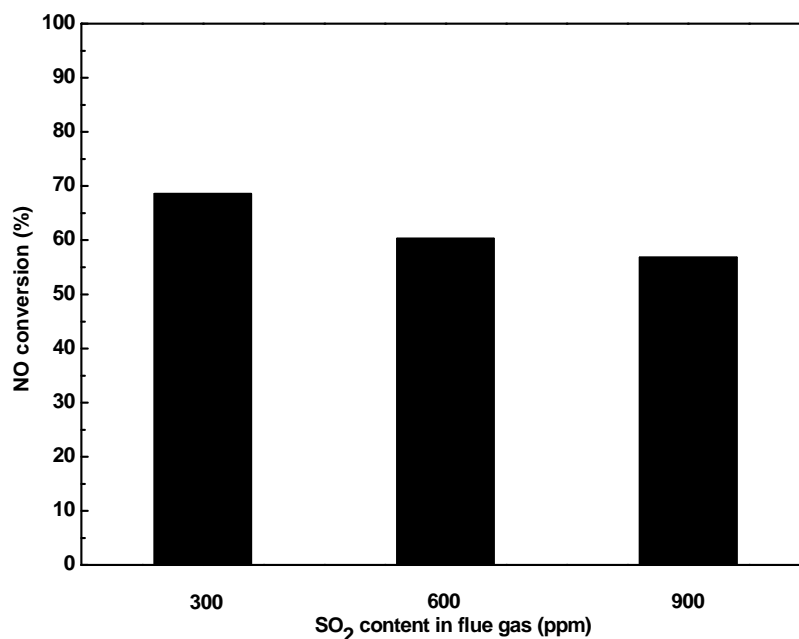
**Fig.7. Effect of the SO₂ concentration on NO conversion of 8% CeO₂/Al-MCM-41**

### CONCLUSION

In this work, the conversion efficiency of NO is investigated over $CeO_2$/Al-MCM-41 at different reaction condition in a lab-scale fixed-bed system. The experimental results show that $CeO_2$ can catalyze the SCR reaction. With the increasing of $CeO_2$ loading value, the NO conversion efficiency of $CeO_2$/Al-MCM-41 can significantly enhance. However, when $CeO_2$ loading value exceeds 8 %, the NO conversion efficiency begins to decrease. Moreover, in the temperature tests, the NO conversion efficiency of $CeO_2$/Al-MCM-41 enhances and then decreases after the reaction temperature aboving 350 ºC because of the generation of $Ce(SO_4)_2$. in the simulated flue gas system of $N_2 + O_2 + SO_2 + NO + NH_3$, the presence of $O_2$ has positive effects on the NO conversion efficiency, while the presence of $SO_2$ has inhibitory effects on the NO conversion efficiency.

### REFERENCES

[1] ZP Zhu; ZY Liu; SJ Liu; HX Niu; TD Hu; T Liu; YN Xie. *Appl. Catal. B: Environ.*, **2000**, 26(1), 25-35.
[2] ZG Lei; CP Wen; BH Chen. *Environ. Sci. Technol.*, **2011**, 45(8), 3437-3444.
[3] Z Si; D Weng; X Wu; R Ran; Z Ma. *Catal. Commun.*, **2012**,17(5),146-149.
[4] H Chang; J Li; X Chen; L Ma; S Yang; JW Schwank; J Hao. *Catal. Commun.*, **2012**, 27(5), 54-57.
[5] WC Yu; XD Wu; ZC Si; D Weng. *Appl. Surf. Sci.*, **2013**, 283(15), 209-214.
[6] L Lietti; I Nova; G Ramis; L Dall'Acqua; G Busca; E Giamello; P Forzatti; F Bregani. *J. Catal.*, 187(2), 419-435.
[7] BX Jiang; Y Liu; Z Wu. *J. Hazard Mater.*, **2009**, 162(2-3),1249-1254.
[8] L Qian; J Zhu; W Du; X Qian. Mater. Chem. Phys., **2009**, 115(2-3), 835-840.
[9] L Chen; J Li; M Ge. *J. Phys. Chem. C.*, **2009**, 113(50), 21177–21184.
[10] X Gao; Y Jiang; Y Zhong; Z Luo; K Cen. *J. Hazard Mater.*, **2010**, 174(1-3),734-739.
[11] A Holmgren; B Andersson; D Duprez. *Appl. Catal. B-Environ.*, **1999**, 22(3), 215-230.
[12] Y Shen; S Zhu; T Qiu; S Shen. *Catal. Commun.*, **2009**, 11(1), 20-23.
[13] J Li; N Yan; Z Qu; S Qiao; S Yang; Y Guo; P Liu; J Jia. *Environ. Sci. Technol.*, **2010**, 44(1), 426-431.
[14] CT Kresge; ME Leonowicz; WJ Roth; JC Vartuli; JS Beck. *Nature*, **1992**, 359(6397), 710-712.
[15] JS Beck; JC Vartuli; WJ Roth; MELeonowicz; CT Kresge; KD Schmitt ; CTW Chu; DH Olson; EW Sheppard. *J. Am. Chem. Soc.*, **1992**, 114(27),10834-10843.
[16] ZY Wu; HJ Wang; TT Zhuang; LB Sun; YM Wang; JH Zhu. *Adv. Funct. Mater.*,**2007**, 18(1), 82-94.
[17] ZH Luan; CF Cheng; WZ Zhou; J Klinowski. *J. Phys. Chem.*, **2002**, 99(3), 1018-1024.

[18] ZH Luan; CF Cheng; WZ Zhou; J Klinowski. *J. Am. Chem. Soc.*,**2001**, 123(21), 5014-5021**.**
[19] X Zhao; GQ (Max) Lu; GJ Millar. *Ind. Eng. Chem. Res.*, **1996**, 35(7), 2075-2090.
[20] R Ryoo; HK Chang; RF Howe. *Chem. Mater.*, **1997**, 9(7), 1607-1613.
[21] R Mokaya .*Adv. Mater.*, **2000**, 12(22), 1681-1685.
[22] C Huo; J Ouyang; H Yang. *Sci. Rep.*, **2014**, 4(2), 3682-3682.
[23] Z Mei; Z Shen; Q Zhao; W Wang; Y Zhang. *J. Hazard Mater.*, **2008**, 152(2), 721-729.
[24] H Li; C Wu; Y Li; J Zhang. *Appl. Cata.l B-Environ.*, **2012**, 111-112(12), 381-388.
[25] Yu Q; Zhang S; Wang X; Lu Z. *Clean Coal Technol.*, **2007**, 13(3), 76-79.
[26] H Zhu, M Shen; T Liu; S Wei; Y Hu; L Dong; Y Chen. *Chinese J. Catal.*, **2002**, 23(4), 325-328.